

Modelling for Poisson process intensities over irregular spatial domains

Chunyi Zhao and Athanasios Kottas

Department of Statistics, University of California, Santa Cruz

June 10, 2021

Abstract

We develop nonparametric Bayesian modelling approaches for Poisson processes, using weighted combinations of structured beta densities to represent the point process intensity function. For a regular spatial domain, such as the unit square, the model construction implies a Bernstein-Dirichlet prior for the Poisson process density, which supports general inference for point process functionals. The key contribution of the methodology is two classes of flexible and computationally efficient models for spatial Poisson process intensities over irregular domains. We address the choice or estimation of the number of beta basis densities, and develop methods for prior specification and posterior simulation for full inference about functionals of the point process. The methodology is illustrated with both synthetic and real data sets.

KEY WORDS: Bayesian nonparametrics; Bernstein-Dirichlet process prior; Markov chain Monte Carlo; Non-homogeneous Poisson process.

1 Introduction

There has been an increasing interest in extracting information from locations in spatial data. For spatial point patterns, both the number and the locations of points are random. Point pattern data is modelled as a realization, within compact domain \mathcal{D} , of a point process whose finite dimensional distribution defines the stochastic mechanism for the number and locations of the points. Independent increments along with a Poisson distributional assumption define the Poisson process. A homogeneous Poisson process is equivalent to complete spatial randomness, that is, the point pattern generated is independently and identically uniformly distributed over \mathcal{D} . The practically relevant version is the non-homogeneous Poisson process (NHPP), which allows the point process intensity to differ by location. The NHPP is characterized by a non-negative, locally integrable intensity function $\lambda(s)$, such that: for any bounded subset \mathcal{B} of the domain, the number of points in \mathcal{B} , $N(\mathcal{B})$, is Poisson($\int_{\mathcal{B}} \lambda(s) ds$) distributed; and, given $N(\mathcal{B})$, the point locations within \mathcal{B} are independent and identically distributed with density $\lambda(s) / \int_{\mathcal{B}} \lambda(u) du$. Therefore, the NHPP likelihood corresponding to point pattern $\{s_1, \dots, s_n\}$, observed in compact domain \mathcal{D} , can be expressed

as:

$$p(\{s_1, \dots, s_n\}; \lambda(s)) \propto \exp\left(-\int_{\mathcal{D}} \lambda(s) ds\right) \prod_{i=1}^n \lambda(s_i) \quad (1)$$

where $n \equiv N(\mathcal{D})$. We consider the more common settings where $\mathcal{D} \subset \mathbb{R}$ or $\mathcal{D} \subset \mathbb{R}^2$. We place particular emphasis on spatial NHPPs, and more specifically on building flexible, computationally tractable models for spatial intensities defined over domains with irregular shapes.

Theoretical study of NHPPs can be found in Cressie (1993) and Daley & Vere-Jones (2008), among other references. Diggle (2003) provides background on likelihood and classical nonparametric inference for spatial NHPPs. Moller & Waagepetersen (2003) discuss simulation-based inference for point processes. Regarding model-based methods for NHPPs, Gelfand & Schliep (2018) categorize the main approaches in two general directions: modelling the trend surface for the intensity function $\lambda(s)$; and, factorizing the intensity function into the total intensity, $\Lambda = \int_{\mathcal{D}} \lambda(s) ds$, and the NHPP density $f(s) = \lambda(s)/\Lambda$, and modelling each separately.

The early Bayesian nonparametric approaches fall under the first category, focusing on modelling temporal NHPP cumulative intensity functions, $\int_0^t \lambda(s) ds$, with gamma, beta or general Lévy process priors (Lo, 1982, 1992). The next stage in this line of research involves mixture models for NHPP intensities built from non-negative kernels convolved with weighted gamma processes (Lo & Weng, 1989; Wolpert & Ickstadt, 1998; Ishwaran & James, 2004; Kang et al., 2014). Also in this direction are modelling approaches based on log-Gaussian Cox processes (Moller et al., 1998) under which the logarithm of the intensity function is a realization of a Gaussian process. Adams et al. (2009) proposed a related approach based on a logistic instead of logarithmic transformation to link the Gaussian process with the model for the intensity function. Modelling directly the intensity function $\lambda(s)$ brings computational challenges for full posterior inference due to the likelihood normalizing term, $\exp(-\int_{\mathcal{D}} \lambda(s) ds)$, especially under methods based on Gaussian process priors. Such challenges have been addressed through approximations of the stochastic integral (Brix & Moller, 2001; Brix & Diggle, 2001), data augmentation (Adams et al., 2009), and discretization of the observation domain \mathcal{D} (Illian et al., 2012).

Under the second direction, Kottas (2006) and Kottas & Sansó (2007) proposed an approach that connects the NHPP intensity function with the density function supported on the observation domain, and models the NHPP density with Dirichlet process mixture priors for density estimation. Taddy & Kottas (2012) extend this modelling approach to marked Poisson processes, and Taddy (2010), Kottas et al. (2012), Xiao et al. (2015) and Rodriguez et al. (2017) develop hierarchical and dynamic models for NHPPs in the context of specific applications. This modelling approach enables an inference framework that builds from well established methods for Dirichlet process mixtures, avoiding the computational challenges due to the NHPP likelihood normalizing component. However, it relies on a potentially restrictive prior structure that models separately the NHPP density and the total intensity over the observation domain.

Inference methods for irregular domain spatial point process intensities have received limited attention in the Bayesian nonparametrics literature. We are only aware of the log-Gaussian Cox process approach of Simpson et al. (2016). Here, the irregular domain adds an extra level of complexity, which has been handled with an approximation to the Gaussian random field, an associated approximation to the NHPP likelihood, and using integrated nested Laplace approximation for fast, but approximate Bayesian inference.

Our main contribution is flexible modelling and computationally efficient inference for NHPPs over spatial domains with irregular shapes. The proposed models do not rely on approximations of the NHPP likelihood and they can be efficiently implemented with standard Markov chain Monte Carlo algorithms for full Bayesian inference and uncertainty quantification. Moreover, in the context of the more commonly studied setting of spatial NHPPs over regular domains, our modelling approach overcomes some of the limitations of existing Bayesian methods, while retaining the feature of flexible inference for general intensity shapes.

We build the model for the NHPP intensity function from weighted combinations of Bernstein polynomial basis functions, that is, beta densities with specified shape parameters. Such parsimonious mixture representation is the key to achieve computationally tractable inference. In Section 3, we explore two modelling approaches for spatial Poisson process intensities over irregular domain, taken without loss of generality to be a subset of the unit square. Under the first approach, the representation for the NHPP intensity is motivated by truncating over the irregular domain a NHPP density defined as a weighted combination of Bernstein densities on the unit square. The second approach targets directly the NHPP intensity modelling it as a structured weighted combination of truncated Bernstein densities. The two models offer different benefits while sharing the feature that the total intensity, Λ , can be readily expressed in terms of model parameters. Thus, both models bypass the challenge brought about from the NHPP likelihood normalizing term without separating the total intensity and NHPP density in the prior specification. In the case of regular domain, say the unit square, the two modelling approaches yield the same form for the NHPP intensity which implies a Bernstein-Dirichlet prior for the corresponding NHPP density. To highlight this connection and its implications in posterior simulation, we begin in the next section with the methodology for the simpler setting of temporal NHPPs.

2 Methodology for temporal Poisson processes

2.1 Model formulation

Here, we focus on modelling one-dimensional NHPPs observed over a bounded domain, taken without loss of generality to be the unit interval. Motivated by Bernstein polynomial priors for densities with bounded support, our model for the intensity function $\lambda(s)$ implies a Bernstein-Dirichlet process prior for the NHPP density, $f(s) = \lambda(s) / \int_0^1 \lambda(u) du$, for $s \in [0, 1]$.

The Bernstein polynomial prior model for density f on $[0, 1]$ is given by $f_K(s | F) = \sum_{k=1}^K \omega_k \text{be}(s | k, K - k + 1)$, where $\text{be}(\cdot | a, b)$ is the beta density with mean $a/(a + b)$. The mixture weights are defined through increments of a distribution function F with support on $[0, 1]$, such that $\omega_k = F(k/K) - F((k - 1)/K)$, for $k = 1, \dots, K$. A distribution F with flexible shape implies mixture weights that select the appropriate beta basis densities to achieve general shapes for density f . This motivates assigning a nonparametric prior to F , such as the Dirichlet process prior (Ferguson, 1973) which results in the Bernstein-Dirichlet prior for density f (Petrone, 1999a,b). Theoretical support for the Bernstein polynomial model is provided by the fact that, as $K \rightarrow \infty$, $f_K(s | F)$ converges uniformly to the density of F (Levasseur, 1984); this result is also key to establishing Kullback-Leibler support and posterior consistency of the Bernstein-Dirichlet prior for density estimation (Petrone & Wasserman, 2002). Extensions of Bernstein polynomial prior models include density estimation on higher dimensional spaces (Zheng et al., 2010; Barrientos

et al., 2015) and density regression (Barrientos et al., 2017).

Our modelling approach is motivated by the structure of the distribution for the mixture weights, $(\omega_1, \dots, \omega_K)$, implied by a Dirichlet process prior, $\text{DP}(\alpha, F_0)$, on F , where α is the Dirichlet process precision parameter, and F_0 the centering distribution with support on $[0, 1]$. Based on the Dirichlet process definition, $(\omega_1, \dots, \omega_K)$, given α, F_0 , and K , follows a Dirichlet $(\alpha A_1, \dots, \alpha A_K)$ prior distribution, where $A_k = F_0(k/K) - F_0((k-1)/K)$, for $k = 1, \dots, K$. The key observation for the model is that the prior distribution for $(\omega_1, \dots, \omega_K)$ can be constructed through independent gamma random variables. In particular, denoting by $\text{Ga}(a, b)$ the gamma distribution with mean a/b , we have $\omega_k = V_k / \{\sum_{r=1}^K V_r\}$, where, for $k = 1, \dots, K$, the V_k are independently $\text{Ga}(\alpha A_k, C)$ distributed, with $C > 0$ a constant.

The proposed model for one-dimensional NHPP intensities is given by:

$$\lambda(s) = \sum_{k=1}^K V_k \text{be}(s \mid k, K - k + 1), \quad s \in [0, 1] \quad (2)$$

$$V_k \mid \alpha, F_0 \stackrel{\text{ind.}}{\sim} \text{Ga}(\alpha \{F_0(k/K) - F_0((k-1)/K)\}, C), \quad k = 1, \dots, K.$$

The total intensity over the domain is $\Lambda = \int_0^1 \lambda(u) du = \sum_{k=1}^K V_k$, and thus the NHPP density is given by $f(s) = \lambda(s) / \{\int_0^1 \lambda(u) du\} = \sum_{k=1}^K \omega_k \text{be}(s \mid k, K - k + 1)$, where $\omega_k = V_k / \{\sum_{r=1}^K V_r\}$. Hence, the implied model for the NHPP density is the Bernstein-Dirichlet prior model. Based on the Dirichlet process definition, this connection holds true for any K , that is, for any partition $\{S_k = [(k-1)/K, k/K) : k = 1, \dots, K\}$ of the unit interval.

Note that, since $\Lambda = \sum_{k=1}^K V_k$, we have $E(\Lambda \mid \alpha) = \alpha/C$, which justifies using a general constant C in the prior for the V_k , rather than taking $C = 1$. That is, we wish to avoid the conflict of large values of α that would be needed under $C = 1$ for large prior expected total intensity versus small values of α favoring non-standard intensity function shapes.

A $\text{Ga}(a_\alpha, b_\alpha)$ prior is assigned to α . In terms of model economy, the uniform distribution is an appealing choice for F_0 . This choice is sufficiently flexible in practice, as shown with the data examples of Section 2.3, and it also yields a form for the average intensity that facilitates prior specification. With F_0 uniform, the prior mean for the intensity is constant, given by $E(\alpha)/C$, and it does not depend on K . Details on the prior mean for the intensity function are provided in the Appendix.

To explore posterior simulation under model (2), we consider two equivalent hierarchical model formulations for the observed point pattern $\{0 < s_1 < \dots < s_n < 1\}$. As discussed above, there is an one-to-one correspondence between parameter vectors (V_1, \dots, V_K) and $\{\Lambda, (\omega_1, \dots, \omega_K)\}$, where $\omega_k = F(S_k)$, for $k = 1, \dots, K$. The prior distribution for (V_1, \dots, V_K) in (2) corresponds to a $\text{DP}(\alpha, F_0)$ prior for F , and a $\text{Ga}(\alpha, C)$ prior for Λ . Moreover, the NHPP likelihood in (1) can be conveniently expressed in terms of either parameterization:

$$\prod_{k=1}^K e^{-V_k} \prod_{i=1}^n \left\{ \sum_{k=1}^K V_k \text{be}(s_i \mid k, K - k + 1) \right\} = e^{-\Lambda} \Lambda^n \prod_{i=1}^n \left\{ \sum_{k=1}^K F(S_k) \text{be}(s_i \mid k, K - k + 1) \right\}.$$

Working with fixed K , the intensity formulation involves parameters $\{(V_1, \dots, V_K), \alpha\}$. Here, we introduce discrete latent variables $\{\xi_i : i = 1, \dots, n\}$ indicating basis configuration for each time event. In a Gibbs sampler setting, the posterior full conditional for each ξ_i is a discrete distribution with support on $\{1, \dots, K\}$. Most importantly, given $\{\xi_i : i = 1, \dots, n\}$ and α , each

V_k follows a gamma posterior full conditional distribution, independently of $\{V_r : r \neq k\}$. Lastly, α can be sampled using a Metropolis-Hastings step.

Alternatively, the density formulation builds from parameters $\{\Lambda, F, \alpha, K\}$. In this case, we introduce continuous latent variables $\{\theta_i : i = 1, \dots, n\}$ to leverage the Dirichlet process mixture representation for the NHPP density function:

$$f(s_i) \equiv f_K(s_i | F) = \int \sum_{k=1}^K \mathbb{1}_{[\frac{k-1}{K}, \frac{k}{K})}(\theta_i) \text{be}(s_i | k, K - k + 1) dF(\theta_i). \quad (3)$$

A practically important feature of this formulation is that the number of basis densities, K , can be estimated without resorting to trans-dimensional Markov chain Monte Carlo algorithms. Here, the dimension of the parameter space does not change with K because the posterior distribution does not involve the weights ω_k , but rather the random distribution F whose increments define the mixture weights. Posterior simulation proceeds by first sampling from the marginal posterior of $\{(\theta_1, \dots, \theta_n), \Lambda, \alpha, K\}$, using Markov chain Monte Carlo methods for Dirichlet process mixtures (Escobar & West, 1995; Neal, 2000). We then sample $(\omega_1, \dots, \omega_K)$, given $(\theta_1, \dots, \theta_n), \alpha, K$, from the Dirichlet distribution implied by the Dirichlet process conditional posterior distribution for F , given $(\theta_1, \dots, \theta_n)$ and α . Finally, posterior samples for the NHPP density and intensity can be readily obtained, using their expressions under model (2). Full details for both posterior simulation algorithms are given in the Appendix.

2.2 Prior specification

The prior for α and the value for C can be specified using prior guesses at the total intensity, $\hat{\Lambda}$, and an average intensity value, $\hat{\lambda}$, over the observation window. We select b_α to provide a wide range for α , and using $E(\lambda(s)) = E(\alpha)/C$, set $E(\alpha) = a_\alpha/b_\alpha = C\hat{\lambda}$. The marginal prior for the total intensity is $p(\Lambda) = \int \text{Ga}(\Lambda | \alpha, C) \text{Ga}(\alpha | b_\alpha C \hat{\lambda}, b_\alpha) d\alpha$. We use this expression to specify C such that the median of $p(\Lambda)$ is equal to $\hat{\Lambda}$.

Note the connection between α and K in controlling the shape of prior realizations for the NHPP intensity: for fixed α , increasing K results in intensities with larger number of modes and more local features; and, for fixed K , decreasing α favors more variability and more localized structure in the intensities. In practice, it may suffice to estimate only α keeping K fixed at sufficiently large values. Note that the beta densities in model (2) play the role of basis functions rather than of kernel densities in finite mixture models. Also key is the Dirichlet process underlying the prior for the weights V_k , which select the subset of beta densities that contribute more to the intensity representation. As illustrated with simulated data in Section 2.3, the discrete nature of the Dirichlet process prior can effectively guard against over-fitting if one conservatively chooses a larger value for K than may be necessary for a particular point pattern.

A possible approach to specify K involves prior information on the peak of the intensity, $\hat{\lambda}_{\max}$, without necessarily knowing where in the observation window the peak occurs. The idea is to find K such that $\hat{\lambda}_{\max}$ matches a percentile of the prior distribution of b^*V_{\max} , where $V_{\max} = \max\{V_k : k = 1, \dots, K\}$, and b^* is the modal value of the beta(2, $K - 1$) density, that is, the first member of the Bernstein polynomial basis with a unimodal density. Under the uniform F_0 distribution, the V_k are independently and identically gamma distributed, and thus the prior distribution of V_{\max} is analytically available given α ; the marginal prior for V_{\max} can also be readily explored through simulation. Table 1 provides an illustration, using the 90th percentile of the marginal prior

Table 1: Illustration of the prior specification strategy for K . $Q_{0.9}^{V_{\max}}$ denotes the 90th percentile of the marginal prior distribution for $\max\{V_k : k = 1, \dots, K\}$, and b^* the modal value of the $\text{beta}(2, K - 1)$ basis density.

K	$Q_{0.9}^{V_{\max}}$	b^*	$b^* \times Q_{0.9}^{V_{\max}}$
20	232.34	7.56	1755.85
30	208.18	11.23	2338.0
50	181.36	18.58	3370.34
100	167.38	36.97	6188.82

distribution for V_{\max} , under a $\text{Ga}(2.53, 0.1)$ prior for α , and with values for the peak intensity that are relevant to one of the data examples of Section 2.3.

As discussed in Section 2.1, using the intensity formulation, with fixed K , allows for a particularly simple and efficient method to implement model (2). The more general version of the model with random K can be implemented at the expense of somewhat more complex Markov chain Monte Carlo algorithms for Dirichlet process mixtures. A discrete uniform or a truncated Poisson distribution with support on $[K_{\min}, K_{\max}]$ are possible priors for K .

2.3 Synthetic data examples for the temporal NHPP model

We consider two synthetic data sets generated from NHPPs with bimodal intensities. For the first example, the intensity is $\lambda(s) = 700 \text{be}(s | 3, 18) + 300 \text{be}(s | 13, 8)$; this can be viewed as a special case of model (2) with $K = 20$, although our prior model does not allow for zero weights. The second data set is obtained by logit-transforming points generated from a weighted combination of normal densities, $\lambda(s) = 400 \text{N}(s | -2.2, 1.0) + 600 \text{N}(s | 0.3, 0.8)$. We take large sizes for the simulated point patterns – $n = 993$ for the first, and $n = 1037$ for the second example – to ensure a meaningful comparison of posterior estimates with the true intensities.

We follow the approach of Section 2.2 to specify $C = 0.023$ and a $\text{Ga}(2.53, 0.1)$ prior for α , using for both data examples 1000 as the prior estimate for the total intensity, and 1100 for the average intensity. For the first example, we take $K = 20$, as well as $K = 40$ to study the implication of using a number of basis densities that is twice as large as what should suffice. For the second example, assume we are told that the peak of the intensity has a value around 2300. Then, referring to Table 1, $K = 30$ can be taken as the number of basis densities, or, more conservatively, as a lower bound. We consider again a larger value, $K = 50$, to check sensitivity of posterior inference results. We also implemented the density formulation for the second example, with a uniform prior on $[20, 60]$ assigned to K .

As shown in Fig. 1, the model is effective in estimating the weights that drive the bimodal intensity shape of the two-component beta mixture. Under $K = 20$, it gives most weight to V_3 and V_{13} , that correspond to basis densities $\text{be}(s | 3, 18)$ and $\text{be}(s | 13, 8)$, whereas when $K = 40$, the model favors 6-7 basis densities with peaks in the same range as the two modes of the underlying intensity. Hence, the model is able to achieve sparsity in estimation of the mixture weights when a surplus of basis densities are used, even though F_0 is a uniform distribution. Moreover, with the

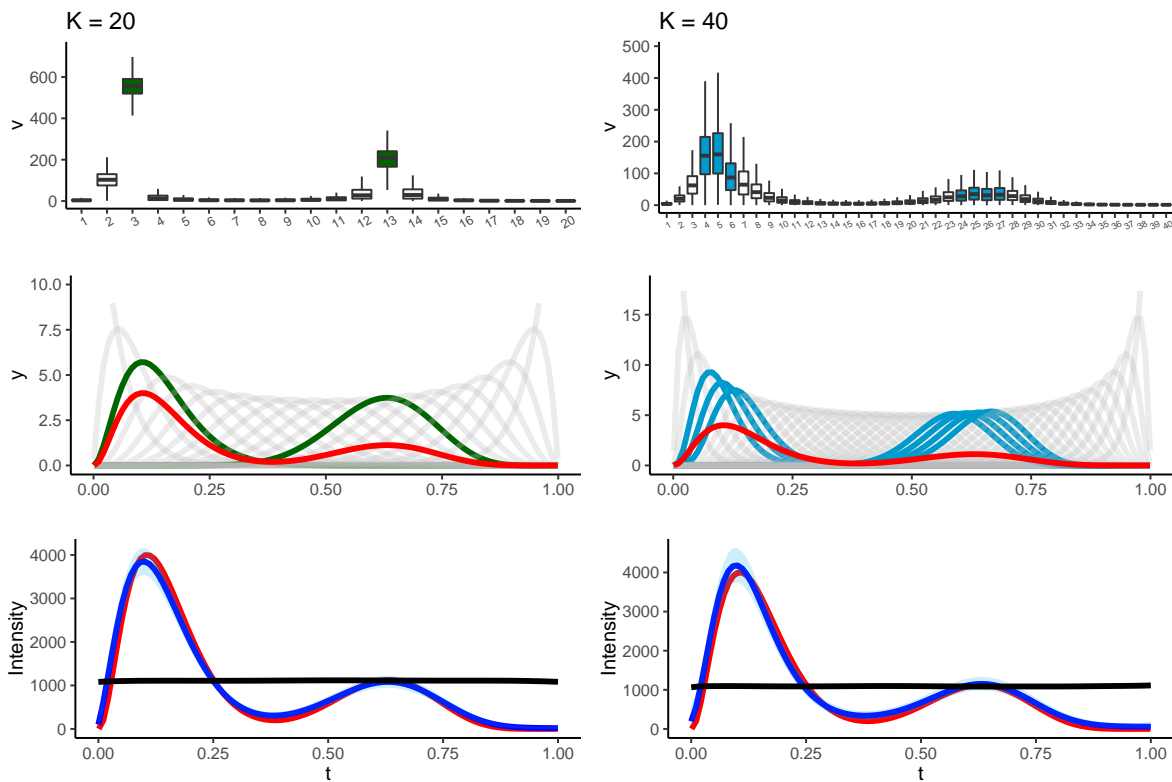


Figure 1: Beta mixture synthetic data example. Results under the intensity formulation with $K = 20$ (left column) and $K = 40$ (right column). Boxplots of posterior samples for the weights V_k (first row), the beta basis densities corresponding to the largest V_k (second row), and posterior mean (blue line) and 95% interval estimates (light blue shaded bands) for the intensity function (third row). In the second and third rows, the red line denotes the true density and intensity, respectively. In the third row, the black line indicates the prior mean for the intensity function.

exception of some increase in the width of posterior uncertainty bands, inference results for the intensity function are similar under the two different choices for K .

This is also the case with the posterior inference results for the logit-normal mixture data example; see Fig. 2. Under the density formulation, the posterior median for K is 36, with the 95% credible interval given by [22, 56]. The intensity function under random K has similar point estimate and a slightly tighter uncertainty band compared to that under $K = 50$.

3 Modelling approaches for Spatial Poisson processes

We begin with the case of a regular domain for the spatial NHPP, taken without loss of generality to be the unit square, such that $s \equiv (x, y) \in [0, 1]^2$. The extension of the Bernstein polynomial basis consists of products of beta densities. More specifically, the basis density with index (k_x, k_y) , for $k_x, k_y = 1, \dots, K$, is defined as

$$\phi_{k_x, k_y}(x, y) = \text{be}(x \mid k_x, K - k_x + 1) \text{be}(y \mid k_y, K - k_y + 1), \quad (x, y) \in [0, 1]^2. \quad (4)$$

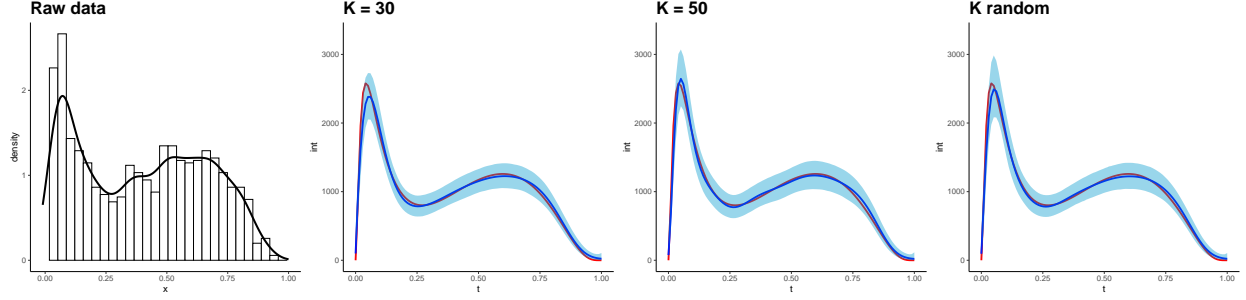


Figure 2: Logit-normal mixture synthetic data example. From left to right, histogram of the simulated time points, and posterior mean (blue line) and 95% interval estimates (light blue shaded bands) for the intensity function under $K = 30$, $K = 50$, and K random. The red line in the last three panels denotes the true intensity.

Although the number of basis densities may be different in the x and y dimensions, we use the more parsimonious form with $K_x = K_y = K$.

Then, we can extend model (2) to the following model for spatial NHPP intensities over $[0, 1]^2$:

$$\lambda(x, y) = \sum_{k_x, k_y=1}^K V_{k_x, k_y} \phi_{k_x, k_y}(x, y), \quad (x, y) \in [0, 1]^2 \quad (5)$$

$$V_{k_x, k_y} \mid \alpha, F_0 \stackrel{ind.}{\sim} \text{Ga}(\alpha F_0(S_{k_x, k_y}), C), \quad k_x, k_y = 1, \dots, K$$

where $S_{k_x, k_y} = [(k_x - 1)/K, k_x/K] \times [(k_y - 1)/K, k_y/K]$, and $F_0(S_{k_x, k_y})$ is the probability of S_{k_x, k_y} under a specified distribution F_0 on $[0, 1]^2$; in particular, $F_0(S_{k_x, k_y}) = 1/K^2$ under the uniform distribution for F_0 .

Again, the total intensity over the domain is readily obtained as $\Lambda = \int_0^1 \int_0^1 \lambda(x, y) dx dy = \sum_{k_x, k_y=1}^K V_{k_x, k_y}$, and the NHPP density is given by $f(x, y) = \sum_{k_x, k_y=1}^K \omega_{k_x, k_y} \phi_{k_x, k_y}(x, y)$, where $\omega_{k_x, k_y} = V_{k_x, k_y} / \{\sum_{k_x, k_y=1}^K V_{k_x, k_y}\}$. The implied prior distribution for the mixture weights $\{\omega_{k_x, k_y}\}$ corresponds to constructing them through $\omega_{k_x, k_y} = F(S_{k_x, k_y})$, where F is a random distribution on $[0, 1]^2$ assigned a $\text{DP}(\alpha, F_0)$ prior.

We thus retain the connection between the intensity prior model in (5) and the two-dimensional Bernstein-Dirichlet prior model for the NHPP density, as well as the equivalent hierarchical model formulations for the data. Again, the implied $\text{Ga}(\alpha, C)$ prior for Λ ensures the coherence between the intensity and density prior models, the latter comprising parameters $\{\Lambda, F, \alpha, K\}$. Extending the approaches outlined in Section 2.1, posterior simulation can be implemented using either the intensity or density formulation. The prior mean intensity is $E(\lambda(x, y)) = E(\alpha)/C$, and thus the prior specification approach of Section 2.2 can be extended to model (5).

To achieve our main objective of flexible inference for NHPP spatial intensities recorded over irregular domain $\mathcal{D} \subset [0, 1]^2$, we propose two different modelling approaches. Under the first model, presented in Section 3.1, the intensity formulation is motivated by truncating over \mathcal{D} the NHPP density $f(x, y)$ defined on $[0, 1]^2$. The second model, developed in Section 3.2, builds the basis representation for the intensity through the corresponding density which is defined as a mixture of truncated beta densities over \mathcal{D} with weights induced by a random distribution F on \mathcal{D} . In both cases, the Bernstein polynomial prior structure is especially attractive to model spatial

point process intensities over irregular domains, a practically relevant problem that, arguably, has not been fully addressed in the Bayesian nonparametrics literature.

3.1 The intensity model

Under the first modelling perspective, the representation for the NHPP intensity $\lambda_{\mathcal{D}}(x, y)$ over irregular domain \mathcal{D} is revealed by the expression for $f_{\mathcal{D}}(x, y)$, the NHPP density truncated on \mathcal{D} . In particular,

$$f_{\mathcal{D}}(x, y) = \frac{f(x, y)}{\int \int_{\mathcal{D}} f(u, v) \, du dv} = \sum_{k_x, k_y=1}^K \frac{V_{k_x, k_y} B_{k_x, k_y}}{\sum_{k_x, k_y=1}^K V_{k_x, k_y} B_{k_x, k_y}} \phi_{k_x, k_y}^*(x, y), \quad (x, y) \in \mathcal{D} \quad (6)$$

where $B_{k_x, k_y} = \int \int_{\mathcal{D}} \phi_{k_x, k_y}(x, y) \, dx dy$, $\phi_{k_x, k_y}^*(x, y) = \phi_{k_x, k_y}(x, y) / B_{k_x, k_y}$ are the basis densities truncated on \mathcal{D} , and we have used the fact that $\omega_{k_x, k_y} B_{k_x, k_y} / \{\sum_{k_x, k_y=1}^K \omega_{k_x, k_y} B_{k_x, k_y}\} = V_{k_x, k_y} B_{k_x, k_y} / \{\sum_{k_x, k_y=1}^K V_{k_x, k_y} B_{k_x, k_y}\}$. The implied model for the intensity function is:

$$\lambda_{\mathcal{D}}(x, y) = \sum_{k_x, k_y=1}^K V_{k_x, k_y} B_{k_x, k_y} \phi_{k_x, k_y}^*(x, y), \quad (x, y) \in \mathcal{D} \quad (7)$$

where $V_{k_x, k_y} \mid \alpha \stackrel{ind.}{\sim} \text{Ga}(\alpha / K^2, C)$, for $k_x, k_y = 1, \dots, K$, taking the uniform distribution for F_0 , and placing a $\text{Ga}(a_\alpha, b_\alpha)$ prior on α .

Evidently, (5) and (7) agree when \mathcal{D} is the unit square. Note that B_{k_x, k_y} will be small for basis densities with significant mass outside \mathcal{D} . Hence, although model (7) uses all K^2 basis densities, the constants B_{k_x, k_y} provide an additional adjustment to the one applied by the random coefficients V_{k_x, k_y} . The overhead cost of computing the normalizing constants B_{k_x, k_y} is very small, since, with fixed K , they need to be computed only once.

For posterior simulation, we introduce a pair of latent variables, (ξ_i, η_i) , for each point in the spatial point pattern, $\{(x_i, y_i) : i = 1, \dots, n\}$, to identify the corresponding basis density. Then, the hierarchical model for the data can be written as:

$$\begin{aligned} \{(x_i, y_i)\} \mid V, \{(\xi_i, \eta_i)\} &\sim \exp\left(-\sum_{k_x, k_y=1}^K V_{k_x, k_y} B_{k_x, k_y}\right) \prod_{i=1}^n \Lambda_{\mathcal{D}} \phi_{\xi_i, \eta_i}^*(x_i, y_i) \\ (\xi_i, \eta_i) \mid V &\stackrel{i.i.d.}{\sim} \sum_{k_x, k_y=1}^K \frac{V_{k_x, k_y} B_{k_x, k_y}}{\Lambda_{\mathcal{D}}} \delta_{(k_x, k_y)}(\xi_i, \eta_i), \quad i = 1, \dots, n \end{aligned} \quad (8)$$

where $V = \{V_{k_x, k_y} : k_x, k_y = 1, \dots, K\}$, and $\Lambda_{\mathcal{D}}$ is the total intensity over the irregular domain, $\Lambda_{\mathcal{D}} = \int \int_{\mathcal{D}} \lambda_{\mathcal{D}}(x, y) \, dx dy = \sum_{k_x, k_y=1}^K V_{k_x, k_y} B_{k_x, k_y}$.

As with models (2) and (5), the form of the NHPP likelihood normalizing term implied by the intensity model (7) results in efficient posterior simulation with remarkably simple updates for parameters $\{V_{k_x, k_y}\}$; given the (ξ_i, η_i) and α , the V_{k_x, k_y} are conditionally independent and gamma distributed. The Markov chain Monte Carlo posterior simulation algorithm is detailed in the Appendix.

In contrast to models (2) and (5), the NHPP density in (6) does not follow the Bernstein-Dirichlet prior. Consequently, we do not have a Dirichlet process mixture representation for the

hierarchical model for the data, which allows estimating K without trans-dimensional posterior simulation algorithms. Therefore, practical implementation of model (8) requires specifying K . In practice, we recommend sensitivity analysis for the value of K . With K selected, the approach of Section 2.2 can be used to specify the prior for α and the value for C . The prior mean of the intensity function is again given by $E(\lambda_{\mathcal{D}}(x, y)) = E(\alpha)/C$, and, although $\Lambda_{\mathcal{D}}$ no longer follows a gamma prior distribution, given α , its marginal prior can be easily developed by simulation.

3.2 The density model

Here, we seek to develop a model for the irregular domain intensity that corresponds to a Bernstein-Dirichlet prior for the associated density, in the spirit of models (2) and (5). To this end, we define directly the density $f_{\mathcal{D}}(x, y)$ as a mixture of truncated beta basis densities:

$$f_{\mathcal{D}}(x, y) = \sum_{(k_x, k_y) \in J_K} \omega_{k_x, k_y}^* \phi_{k_x, k_y}^*(x, y), \quad (x, y) \in \mathcal{D} \quad (9)$$

where $J_K = \{(k_x, k_y) : S_{k_x, k_y} \cap \mathcal{D} \neq \emptyset\}$ is the index set for all non-empty intersections, $S_{k_x, k_y}^* = S_{k_x, k_y} \cap \mathcal{D}$, of the unit square partitioning sets $\{S_{k_x, k_y} : k_x, k_y = 1, \dots, K\}$ with \mathcal{D} . The mixture weights are defined as $\omega_{k_x, k_y}^* = F(S_{k_x, k_y}^*)$, where F is a random distribution on \mathcal{D} following a $\text{DP}(\alpha, F_0)$ prior, with F_0 taken to be the uniform distribution on \mathcal{D} .

We now define the model for the irregular domain spatial intensity as

$$\begin{aligned} \lambda_{\mathcal{D}}(x, y) &= \sum_{(k_x, k_y) \in J_K} V_{k_x, k_y}^* \phi_{k_x, k_y}^*(x, y), \quad (x, y) \in \mathcal{D} \\ V_{k_x, k_y}^* &| \alpha \stackrel{i.i.d.}{\sim} \text{Ga}(\alpha F_0(S_{k_x, k_y}^*), C), \quad (k_x, k_y) \in J_K \end{aligned} \quad (10)$$

such that the density $f_{\mathcal{D}}(x, y) = \lambda_{\mathcal{D}}(x, y) / \{\int \int_{\mathcal{D}} \lambda_{\mathcal{D}}(u, v) du dv\}$ follows the prior model in (9). Again, the key link between parameterizations $\{V_{k_x, k_y}^* : (k_x, k_y) \in J_K\}$ and $\{\Lambda_{\mathcal{D}}, \{\omega_{k_x, k_y}^* : (k_x, k_y) \in J_K\}\}$ is the practical expression for the total intensity $\Lambda_{\mathcal{D}} = \int \int_{\mathcal{D}} \lambda_{\mathcal{D}}(x, y) dx dy = \sum_{(k_x, k_y) \in J_K} V_{k_x, k_y}^*$, and its $\text{Ga}(\alpha, C)$ prior implied by (10).

For a spatial point pattern $\{(x_i, y_i) : i = 1, \dots, n\}$ recorded over \mathcal{D} , we can write the NHPP likelihood in terms of either the intensity of density formulation:

$$\begin{aligned} &\exp\left(-\sum_{(k_x, k_y) \in J_K} V_{k_x, k_y}^*\right) \prod_{i=1}^n \left\{ \sum_{(k_x, k_y) \in J_K} V_{k_x, k_y}^* \phi_{k_x, k_y}^*(x_i, y_i) \right\} \\ &= \exp(-\Lambda_{\mathcal{D}}) \Lambda_{\mathcal{D}}^n \prod_{i=1}^n \left\{ \sum_{(k_x, k_y) \in J_K} F(S_{k_x, k_y}^*) \phi_{k_x, k_y}^*(x_i, y_i) \right\}. \end{aligned}$$

To explore the posterior distribution for $\{\Lambda_{\mathcal{D}}, F, \alpha, K\}$ under the density formulation, we introduce bivariate continuous latent variables $\{z_i\}$ to write the hierarchical model for the data:

$$\begin{aligned} \{(x_i, y_i)\} &| \{z_i\}, \Lambda_{\mathcal{D}}, K \sim \exp(-\Lambda_{\mathcal{D}}) \Lambda_{\mathcal{D}}^n \prod_{i=1}^n \left\{ \sum_{(k_x, k_y) \in J_K} \mathbb{1}_{S_{k_x, k_y}^*}(z_i) \phi_{k_x, k_y}^*(x_i, y_i) \right\} \\ z_i &| F \stackrel{i.i.d.}{\sim} F, \quad i = 1, \dots, n \\ F &| \alpha \sim \text{DP}(\alpha, F_0) \end{aligned} \quad (11)$$

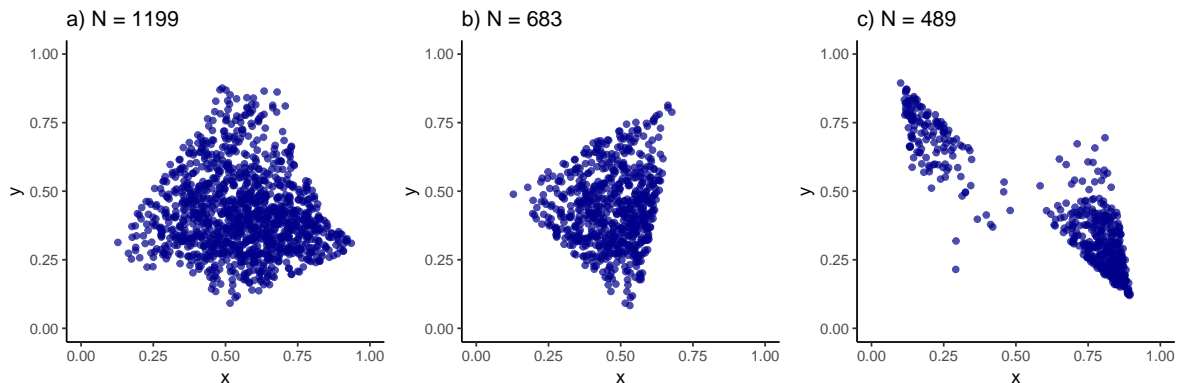


Figure 3: Synthetic spatial point patterns for the irregular domain simulation study. The size of each point pattern is shown in the corresponding panel.

where $\Lambda_{\mathcal{D}} \mid \alpha \sim \text{Ga}(\alpha, C)$, with a $\text{Ga}(a_{\alpha}, b_{\alpha})$ prior placed on α , and with a discrete uniform or a truncated Poisson prior distribution for K with support on $[K_{\min}, K_{\max}]$. The Markov chain Monte Carlo algorithm for model (11) is given in the Appendix. The posterior simulation method is more involved than the one for the intensity model of Section 3.1, but it allows for estimation of K without trans-dimensional computational techniques.

The marginal prior for the total intensity is $p(\Lambda_{\mathcal{D}}) = \int \text{Ga}(\Lambda_{\mathcal{D}} \mid \alpha, C) \text{Ga}(\alpha \mid a_{\alpha}, b_{\alpha}) d\alpha$. Under model (10), there is no closed-form expression for $E(\lambda_{\mathcal{D}}(x, y))$, but $E(\alpha)/C$ is an approximate lower bound for the prior mean intensity. With this caveat, the approach of Section 2.2 can be used to specify the prior hyperparameters for α and the value for C . The earlier approach to specify K can be used here to guide the choice of the support for the prior on K .

4 Synthetic data examples

We study inference results under both the intensity and density model, using point patterns generated under three different scenarios for the irregular shape of the spatial NHPP. The synthetic point patterns are plotted in Fig. 3, and the true intensities, as well as their corresponding polygonal domain, are shown in Fig. 4. For cases (a) and (b), the true NHPP density is a mixture of two bivariate logit-normal densities, truncated over the respective domain, which results in a unimodal intensity. Case (c) arises from truncating a mixture of bivariate beta densities that accumulates most of its mass at the $(0, 1)$ and $(1, 0)$ corners of the unit square.

For all three cases, the intensity model (8) is implemented with $C = 0.05$, a $\text{Ga}(2, 0.01)$ prior for α , and with $K = 20$. The posterior mean and uncertainty estimates reported in Fig. 4 demonstrate that the model recovers well the underlying intensity shapes over the different polygons.

We also applied the density model (11), using for all three data sets, a $\text{Ga}(5, 0.1)$ prior for α , $C = 0.01$, and a discrete uniform prior on $[5, 25]$ for K . The posterior probability for K at its posterior mode was: $\Pr(K = 13 \mid \text{data}) = 0.89$ in case (a), $\Pr(K = 12 \mid \text{data}) = 0.99$ in case (b), and $\Pr(K = 9 \mid \text{data}) = 0.81$ in case (c). The posterior mean and uncertainty estimates under the density model were similar to the ones reported in Fig. 4 under the intensity model.

As an additional illustration, we consider a point pattern of size $n = 303$ drawn from a NHPP

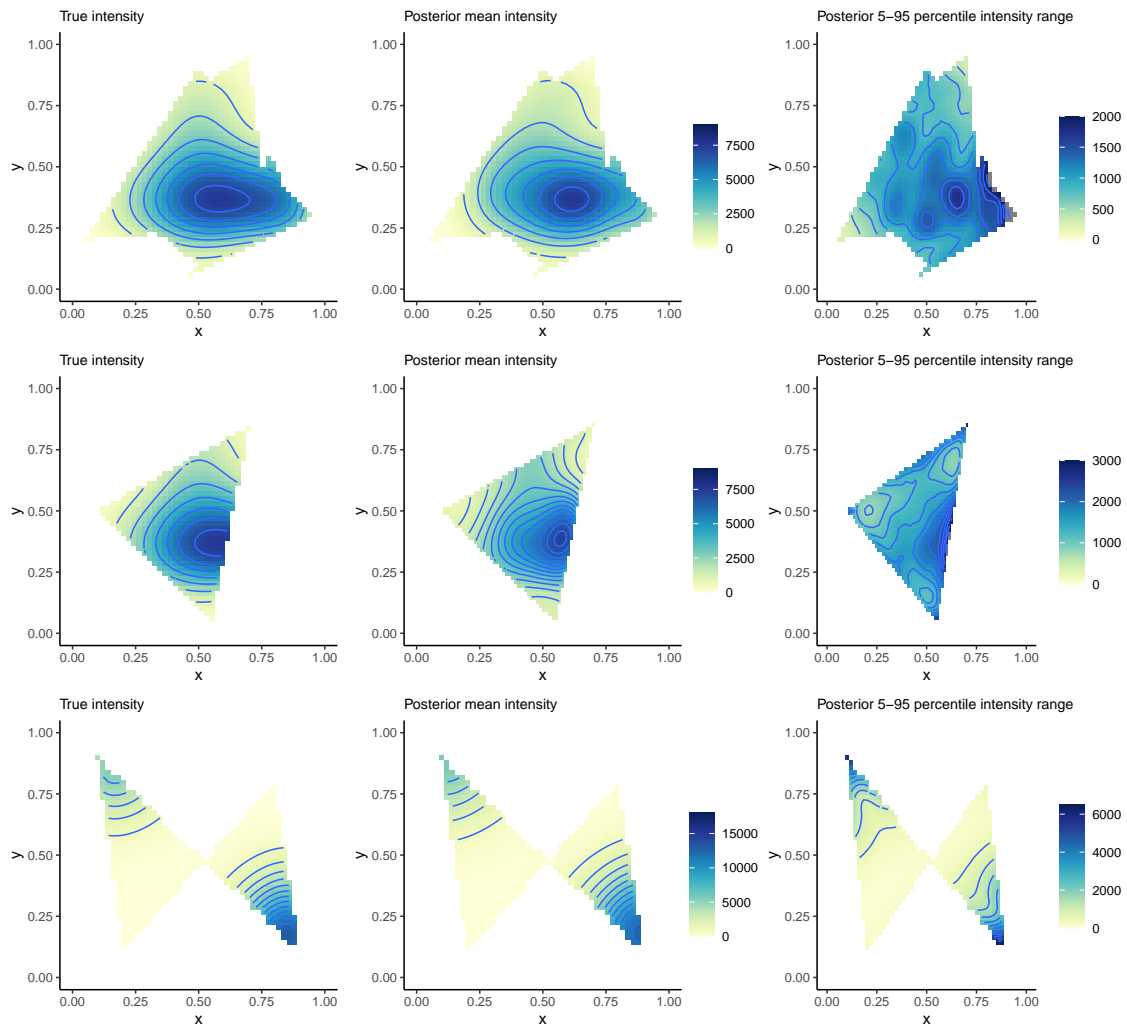


Figure 4: Results for the data in Fig. 3 under the intensity model. The left panel shows the true intensity function, the middle panel the posterior mean intensity estimate, and the right panel a posterior uncertainty estimate in the form of the difference between the 95th and 5th percentiles of the posterior distribution for the intensity function.

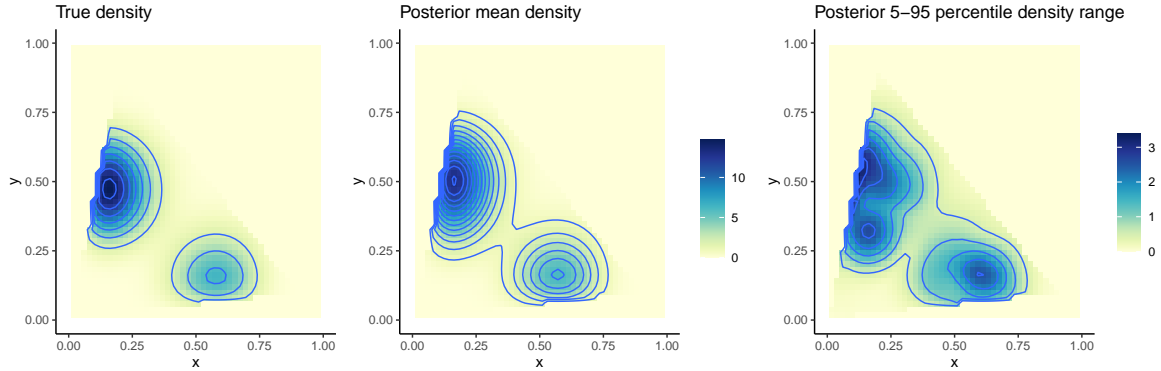


Figure 5: Results for the synthetic spatial point pattern generated from NHPP density $0.7 \text{be}(x \mid 4, 17)\text{be}(y \mid 10, 11) + 0.3 \text{be}(x \mid 12, 9)\text{be}(y \mid 4, 17)$ truncated to the triangle with vertices $\{(0.01, 0.01), (0.2, 0.9), (0.9, 0.1)\}$. The left panel includes the true density. Based on the density model, the middle panel plots the posterior mean density estimate, and the right panel an uncertainty estimate given by the difference between the 95th and 5th percentiles of the posterior distribution of the density function.

with density $0.7 \text{be}(x \mid 4, 17)\text{be}(y \mid 10, 11) + 0.3 \text{be}(x \mid 12, 9)\text{be}(y \mid 4, 17)$ truncated to the triangle with vertices $\{(0.01, 0.01), (0.2, 0.9), (0.9, 0.1)\}$, and with total intensity 300. Here, the truth is designed to resemble the intensity model with $K = 20$, and we test the performance of the density model in estimating K and other NHPP functionals.

Model (11) is implemented with a $\text{Ga}(2, 0.01)$ prior for α , $C = 0.01$, and a discrete uniform prior for K with support on $[15, 25]$. The posterior mean and uncertainty estimates in Fig. 5 show that the underlying bimodal density shape is recovered well, taking into account the moderate size of the point pattern. The posterior mean for the total intensity is 301.1, and the 95% posterior credible interval is given by $(267.3, 334.3)$. The 95% posterior credible interval for K is $[19, 25]$, and the posterior mode is 20, with $\text{Pr}(K = 20 \mid \text{data}) = 0.46$. We note that increasing the size of the simulated point pattern results in posterior distributions for K that are more concentrated around $K = 20$.

5 Boston crime data analysis

For an illustration with real data, we consider the point pattern of $n = 1251$ locations in the city of Boston where vandalism occurred during the second quarter of year 2017; see the top left panel of Fig. 6. In general, spatial point patterns of crime depict more clustering than what a NHPP can model. However, we use such data here to illustrate the spatial NHPP model over a non-trivial irregular domain, including model checking of the NHPP assumption.

The Boston City crime data and the Boston city boundary shape file in longitude and latitude format are publicly available online (Jain, 2018; BostonGIS, 2018). We use the R `rmapshaper` package (Teucher et al., 2021) to smooth this complicated boundary while retaining its key spatial topology. The simplified boundary in the form of Multipolygons is then mapped to a subset of the unit square. To process the raw data, we remove entries with geo-location as NAs, project the

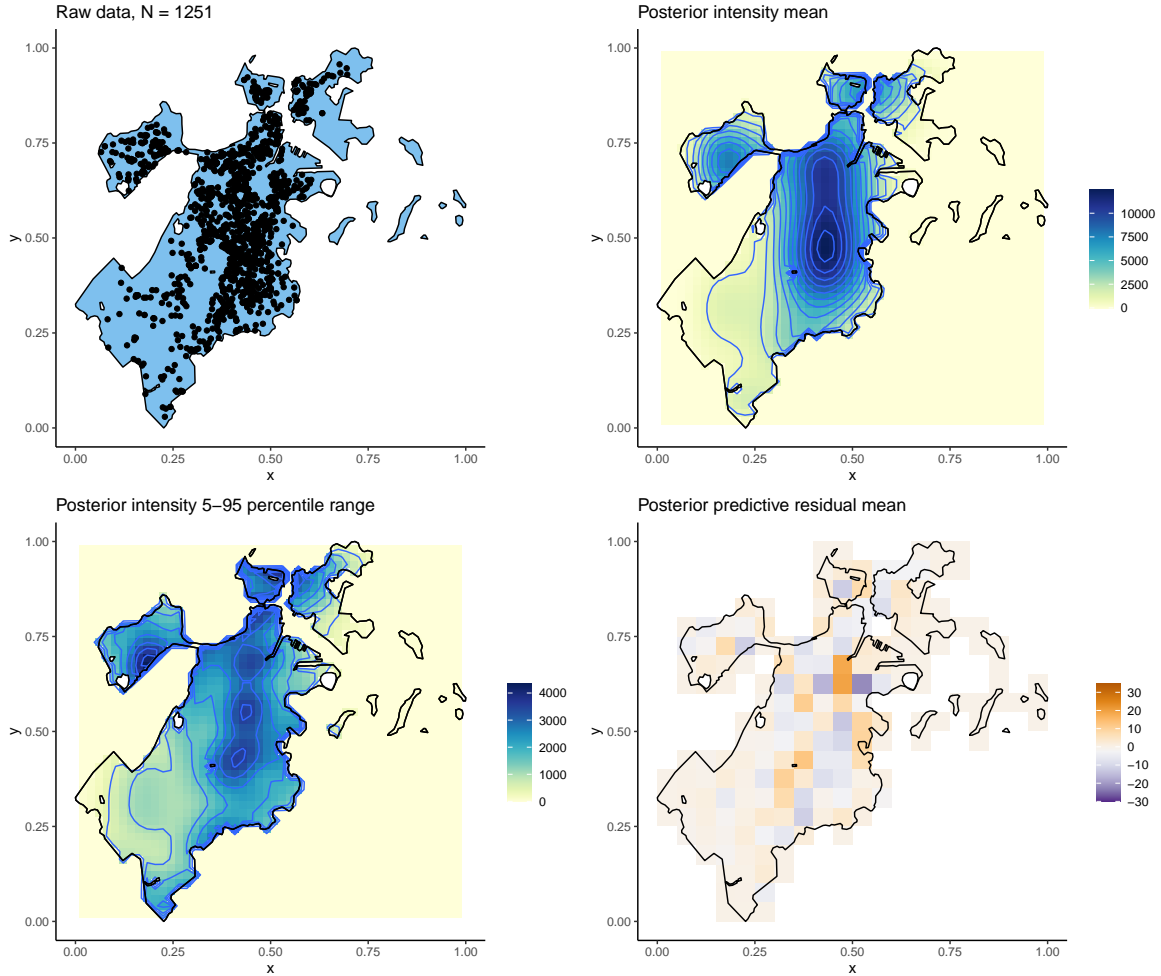


Figure 6: Boston crime data: vandalism in the second quarter of 2017. The observed point pattern is shown in the top left panel. Under the density model, the top right panel plots the posterior mean intensity estimate, and the bottom left panel the difference between the 95th and 5th percentile of the posterior distribution for the intensity function. The bottom right panel plots the posterior mean estimates for the predictive residuals.

vandalism incidence locations from longitude and latitude into Northing and Easting, and finally map the crime locations and city boundary points to the unit square.

We focus on inference results under the density model, implemented with $C = 0.01$, a $\text{Ga}(5, 0.1)$ prior for α , and a truncated Poisson prior for K with mean 20 and support on $[20, 60]$. Fig. 6 plots posterior mean and uncertainty estimates for the intensity of vandalism incidences. The posterior mean for the total intensity of vandalism in the second quarter of 2017 is 1234, with the 95% posterior credible interval given by (1167, 1303). The posterior distribution for K has effective support on $[36, 52]$ and posterior mode at 40 with $\Pr(K = 40 \mid \text{data}) = 0.34$.

For graphical model checking, we consider predictive residuals (Leininger & Gelfand, 2017), defined as $N_{\text{pred}}(\mathcal{B}) - N_{\text{obs}}(\mathcal{B})$, where $N_{\text{obs}}(\mathcal{B})$ and $N_{\text{pred}}(\mathcal{B})$ are respectively the observed and predicted number of points in \mathcal{B} , a subset of the spatial point process domain \mathcal{D} . To sample from the

posterior distribution of $N_{\text{pred}}(\mathcal{B})$, we draw from the Poisson($\int_{\mathcal{B}} \lambda_{\mathcal{D}}(x, y) dx dy$) distribution for each posterior realization of $\lambda_{\mathcal{D}}(x, y)$. In general, lack of fit may be due to the NHPP assumption for the point process that generates the particular point pattern and/or the model used for the NHPP intensity. A flexible prior probability model for the NHPP intensity is practically useful in that it allows focusing discrepancies in the residuals on the NHPP assumption.

To implement model checking with predictive residuals, we create a 20×20 grid over the unit square and select the subset of these 400 square regions that overlap with the Boston city boundary \mathcal{D} as the target regions to cover the entire Boston city. The bottom right panel of Fig. 6 plots the posterior mean estimates for the predictive residuals. The residuals in regions near the city boundary are evaluated based on only the subsets that overlap with \mathcal{D} . This residual analysis suggests a decent fit of the NHPP model. It is perhaps not surprising that the sub-regions with the more pronounced non-zero residual estimates correspond to parts of the city where the data suggest clustering, for which a more general point process than the NHPP would be expected to provide better model fit.

6 Discussion

We have presented two models for spatial NHPP intensities over domains with irregular shapes. To our knowledge, this is the first treatment of this practically relevant problem with methodology that supports general intensity function shapes and allows for full Bayesian inference, while avoiding any type of approximation of the NHPP likelihood.

In the more commonly studied setting of a regular domain, the two modelling approaches result in the same formulation for the NHPP intensity, which corresponds to a Bernstein-Dirichlet prior for the associated NHPP density. Hence, as a useful byproduct of the methodology, we establish a connection between density and intensity estimation under Bernstein-Dirichlet priors. Relative to existing approaches that model directly the intensity function over regular domain, the proposed method arguably offers a substantially more practical inference framework. The prior model for the intensity function can be equivalently represented in terms of a prior for the total intensity over the observation domain and a prior for the density function. In contrast with related existing methods, the priors for the NHPP density and the total intensity are guaranteed to be compatible with the prior for the NHPP intensity.

The two proposed models for spatial NHPPs over irregular domains \mathcal{D} , the intensity model (7) and density model (10), arise from different perspectives. The former model builds from truncating the Bernstein-Dirichlet density model over \mathcal{D} , whereas the latter constructs the irregular domain density as a mixture of truncated beta basis densities. The intensity model uses all K^2 basis densities $\{\phi_{k_x, k_y}^*\}$ and relies on random weights, further adjusted by the normalizing constants B_{k_x, k_y} , to select appropriate basis members in constructing the intensity functional form. The density model is generally more efficient in the intensity representation, as it utilizes a subset of the K^2 basis densities $\{\phi_{k_x, k_y}^*\}$, the size of such subset determined by the particular domain \mathcal{D} . For settings where a value for K can be specified, possibly appealing to empirical experience with synthetic data examples, the intensity model offers the benefit of particularly simple and efficient model fitting. The density model affords more generality in the inference scheme by allowing uncertainty with respect to the number of basis densities, at the cost of a more involved posterior simulation method, which however does not require complex trans-dimensional computational techniques. For both

models, the intensity representation through beta densities with specified parameters is essential for the practicality and computational efficiency of the inference methods for spatial NHPPs over irregular domains.

The proposed methods are also relevant for more general spatial point processes that build from the NHPP to allow hierarchically structured, clustering mechanisms. Current research is exploring Bayesian semiparametric spatial and space-time Hawkes processes for applications where it is important to address the spatial point process irregular domain.

Acknowledgment

This research was supported in part by the National Science Foundation under award SES 1950902.

References

- ADAMS, R. P., MURRAY, I. & MACKAY, D. J. C. (2009). Tractable nonparametric Bayesian inference in Poisson processes with Gaussian process intensities. In *Proceedings of the 26th Annual International Conference on Machine Learning, ICML '09*. New York, NY, USA: ACM.
- BARRIENTOS, A. F., JARA, A. & QUINTANA, F. A. (2015). Bayesian density estimation for compositional data using random Bernstein polynomials. *Journal of Statistical Planning and Inference* **166**, 116–125.
- BARRIENTOS, A. F., JARA, A. & QUINTANA, F. A. (2017). Fully nonparametric regression for bounded data using dependent Bernstein polynomials. *Journal of the American Statistical Association* **112**, 806–825.
- BOSTONGIS (2018). City of Boston Boundary [Shapefile] "Boston Boundary". <https://www.arcgis.com/home/item.html?id=734463787ac44a648fe9119af4e98cae>. 2019-9-19.
- BRIX, A. & DIGGLE, P. J. (2001). Spatiotemporal prediction for log-Gaussian Cox processes. *Journal of the Royal Statistical Society, Series B* **63**, 823–841.
- BRIX, A. & MOLLER, J. (2001). Space-time multi type log Gaussian Cox processes with a view to modelling weeds. *Scandinavian Journal of Statistics* **28**, 471–488.
- CRESSIE, N. A. C. (1993). *Statistics for spatial data*. New York: Wiley.
- DALEY, D. J. & VERE-JONES, D. (2008). *An Introduction to the Theory of Point Processes: Volume II: General Theory and Structure*. Springer, New York, NY.
- DIGGLE, P. (2003). *Statistical Analysis of Spatial Point Patterns*. Arnold.
- ESCOBAR, M. D. & WEST, M. (1995). Bayesian density estimation and inference using mixtures. *Journal of the American Statistical Association* **90**, 577–588.

- FERGUSON, T. S. (1973). A Bayesian analysis of some nonparametric problems. *The Annals of Statistics* **1**, 209–230.
- GELFAND, A. E. & SCHLIEP, E. M. (2018). Bayesian Inference and Computing for Spatial Point Patterns. *NSF-CBMS Regional Conference Series in Probability and Statistics* **10**, i–125.
- ILLIAN, J. B., SØRBYE, S. H. & RUE, H. (2012). A toolbox for fitting complex spatial point process models using integrated nested laplace approximation (INLA). *The Annals of Applied Statistics* **6**, 1499–1530.
- ISHWARAN, H. & JAMES, L. F. (2004). Computational methods for multiplicative intensity models using weighted Gamma processes. *Journal of the American Statistical Association* **99**, 175–190.
- JAIN, A. (2018). Crimes in Boston. <https://www.kaggle.com/ankkur13/boston-crime-data>. 2019-7-10.
- KANG, J., NICHOLS, T. E., WAGER, T. D. & JOHNSON, T. D. (2014). A Bayesian hierarchical spatial point process model for multi-type neuroimaging meta-analysis. *The Annals of Applied Statistics* **8**, 1800–1824.
- KOTTAS, A. (2006). Dirichlet process mixtures of Beta distributions, with applications to density and intensity estimation. In *Proceedings of the Workshop on Learning with Nonparametric Bayesian Methods, 23rd International Conference on Machine Learning*. Pittsburgh, PA, USA.
- KOTTAS, A., BEHSETA, S., MOORMAN, D., POYNOR, V. & OLSON, C. (2012). Bayesian non-parametric analysis of neuronal intensity rates. *Journal of Neuroscience Methods* **203**, 241–253.
- KOTTAS, A. & SANSÓ, B. (2007). Bayesian mixture modeling for spatial poisson process intensities, with applications to extreme value analysis. *Journal of statistical planning and inference* **137**, 3151–3163.
- LEININGER, T. J. & GELFAND, A. E. (2017). Bayesian inference and model assessment for spatial point patterns using posterior predictive samples. *Bayesian Analysis* **12**, 1–30.
- LEVASSEUR, K. M. (1984). A probabilistic proof of the Weierstrass approximation theorem. *The American Mathematical Monthly* **91**, 249–250.
- LO, A. Y. (1982). Bayesian nonparametric statistical inference for Poisson point processes. *Z. Wahrscheinlichkeitstheorie verw. Gebiete* **59**, 55–66.
- LO, A. Y. (1992). Bayesian inference for Poisson process models with censored data. *Journal of Nonparametric Statistics* **2**, 71–80.
- LO, A. Y. & WENG, C.-S. (1989). On a class of Bayesian nonparametric estimates: II. Hazard rate estimates. *Annals of the Institute of Statistical Mathematics* **41**, 227–245.
- MOLLER, J., SYVERSVEEN, A. R. & WAAGEPETERSEN, R. P. (1998). Log Gaussian Cox processes. *Scandinavian Journal of Statistics* **25**, 451–482.

- MOLLER, J. & WAAGEPETERSEN, R. P. (2003). *Statistical Inference and Simulation for Spatial Point Processes*. Chapman and Hall/CRC.
- NEAL, R. (2000). Markov chain sampling methods for Dirichlet process mixture models. *Journal of Computational and Graphical Statistics* **9**, 249–265.
- PETRONE, S. (1999a). Bayesian density estimation using Bernstein polynomials. *The Canadian Journal of Statistics* **27**, 105–126.
- PETRONE, S. (1999b). Random Bernstein polynomials. *Scandinavian Journal of Statistics* **26**, 373–393.
- PETRONE, S. & WASSERMAN, L. (2002). Consistency of Bernstein polynomial posteriors. *Journal of the Royal Statistical Society, Series B* **64**, 79–100.
- RODRIGUEZ, A., WANG, Z. & KOTTAS, A. (2017). Assessing systematic risk in the S&P500 index between 2000 and 2011: A Bayesian nonparametric approach. *The Annals of Applied Statistics* **11**, 527–552.
- SIMPSON, D., ILLIAN, J. B., LINDGREN, F., SØRBYE, S. H. & RUE, H. (2016). Going off grid: computationally efficient inference for log-Gaussian Cox processes. *Biometrika* **103**, 49–70.
- TADDY, M. (2010). Autoregressive mixture models for dynamic spatial Poisson processes: Application to tracking the intensity of violent crime. *Journal of the American Statistical Association* **105**, 1403–1417.
- TADDY, M. A. & KOTTAS, A. (2012). Mixture modeling for marked Poisson processes. *Bayesian Analysis* **7**, 335–362.
- TEUCHER, A., RUSSELL, K. & BLOCH, M. (2021). *rmapshaper: Client for 'mapshaper' for 'Geospatial' Operations*. <https://cran.r-project.org/package=rmapshaper>.
- WOLPERT, R. L. & ICKSTADT, K. (1998). Poisson/gamma random field models for spatial statistics. *Biometrika* **85**, 251–267.
- XIAO, S., KOTTAS, A. & SANSÓ, B. (2015). Modeling for seasonal marked point processes: An analysis of evolving hurricane occurrences. *The Annals of Applied Statistics* **9**, 353–382.
- ZHENG, Y., ZHU, J. & ROY, A. (2010). Nonparametric Bayesian inference for the spectral density function of a random field. *Biometrika* **97**, 238–245.

A Appendix: Prior expectation for the intensity function

We use $\text{be}(\cdot | \cdot, \cdot)$ and $\text{ga}(\cdot | \cdot, \cdot)$ to denote the beta and gamma distributions' probability density functions. We use $\text{Be}(\cdot, \cdot)$ and $\text{Ga}(\cdot, \cdot)$ to denote the Beta and gamma distribution, $\mathbb{1}_{\mathcal{D}}(\mathbf{s})$ to denote the indicator function of whether the point \mathbf{s} in \mathbb{R} or \mathbb{R}^2 is in the interval or region \mathcal{D} . We write the spatial Bernstein basis functions over the unit square as $\phi_{k_x, k_y}(x, y) = \text{be}(x|k_x, K - k_x + 1)\text{be}(y|k_y, K - k_y + 1)$, for $k_x, k_y = 1 \cdots K$, and the spatial Bernstein basis functions over the irregular domain \mathcal{D} as $\phi_{k_x, k_y}^*(x, y) = B_{k_x, k_y}^{-1} \text{be}(x|k_x, K - k_x + 1)\text{be}(y|k_y, K - k_y + 1)$, where B_{k_x, k_y} is the normalizing constant for density ϕ_{k_x, k_y} over the irregular domain \mathcal{D} . We use $\{S_{k_x, k_y} : k_x, k_y = 1 \cdots K\}$ to denote the $K \times K$ unit square partitioning sets, S_{k_x, k_y}^* the overlap between S_{k_x, k_y} and \mathcal{D} , $S_{k_x, k_y}^* = S_{k_x, k_y} \cap \mathcal{D}$, and J_K the index set for S_{k_x, k_y}^* where $S_{k_x, k_y}^* \neq \emptyset$. Finally, we let $F_0(S_{k_x, k_y}^*)$ denote the probability of S_{k_x, k_y}^* under distribution F_0 .

Here, we derive the prior expectation of the intensity function under the different Poisson process models.

For the temporal Poisson process model (2) developed in Section 2.1, we have:

$$\begin{aligned} \mathbb{E}(\lambda(s) | \alpha, K) &= \sum_{k=1}^K \mathbb{E}(V_k | \alpha) \text{be}(s|k, K - k + 1) \\ &= \frac{\alpha}{C} \sum_{k=1}^K \frac{1}{K} \frac{K! s^{k-1} (1-s)^{K-k}}{(k-1)!(K-k)!} \\ &= \frac{\alpha}{C} \sum_{m=0}^{K-1} \frac{(K-1)! s^m (1-s)^{K-1-m}}{m!(K-1-m)!} \\ &= \frac{\alpha}{C} \sum_{m=0}^{K-1} \binom{K-1}{m} s^m (1-s)^{K-1-m} \\ &= \frac{\alpha}{C} \end{aligned}$$

using the Binomial theorem. Note that the conditional prior expectation does not depend on K . Finally, $\mathbb{E}(\lambda(s)) = \mathbb{E}(\mathbb{E}(\lambda(s) | \alpha)) = \mathbb{E}(\alpha)/C$.

For the spatial Poisson process model (5), over the unit square, we can write:

$$\begin{aligned} \mathbb{E}(\lambda(x, y) | \alpha, K) &= \sum_{k_x=1}^K \sum_{k_y=1}^K \mathbb{E}(V_{k_x, k_y} | \alpha) \text{be}(x|k_x, K - k_x + 1)\text{be}(y|k_y, K - k_y + 1) \\ &= \frac{\alpha}{C} \frac{1}{K^2} \sum_{k_x=1}^K \sum_{k_y=1}^K \text{be}(x|k_x, K - k_x + 1)\text{be}(y|k_y, K - k_y + 1) \\ &= \frac{\alpha}{C} \end{aligned}$$

using the fact that $K^{-1} \sum_{m=1}^K \text{be}(s|m, K - m + 1) = 1$, which is essentially a restatement of the Binomial theorem.

Similarly, for the irregular domain spatial model (7), developed in Section 3.1, we obtain:

$$\begin{aligned}
\mathbb{E}(\lambda_{\mathcal{D}}(x, y) \mid \alpha) &= \sum_{k_x=1}^K \sum_{k_y=1}^K B_{k_x, k_y} \mathbb{E}(V_{k_x, k_y} \mid \alpha) \left(B_{k_x, k_y}^{-1} \text{be}(x|k_x, K - k_x + 1) \text{be}(y|k_y, K - k_y + 1) \right) \\
&= \sum_{k_x=1}^K \sum_{k_y=1}^K \mathbb{E}(V_{k_x, k_y} \mid \alpha) \text{be}(x|k_x, K - k_x + 1) \text{be}(y|k_y, K - k_y + 1) \\
&= \frac{\alpha}{C}
\end{aligned}$$

Finally, for the irregular domain spatial model (10), developed in Section 3.2, we do not have an analytical expression for the prior mean intensity function. However, we can obtain an approximate lower bound as follows:

$$\begin{aligned}
\mathbb{E}(\lambda_{\mathcal{D}}(x, y) \mid \alpha, K) &= \sum_{(k_x, k_y) \in J_K} \frac{\alpha F_0(S_{k_x, k_y}^*)}{C} \phi_{k_x, k_y}^*(x, y) \\
&\approx \frac{\alpha}{C} \sum_{(k_x, k_y) \in J_K} \frac{1}{K^2} \phi_{k_x, k_y}^*(x, y) \\
&\geq \frac{\alpha}{C} \sum_{(k_x, k_y) \in J_K} \frac{1}{K^2} B_{k_x, k_y} \phi_{k_x, k_y}^*(x, y) \\
&\approx \frac{\alpha}{C} \sum_{k_x=1}^K \sum_{k_y=1}^K \frac{1}{K^2} B_{k_x, k_y} \phi_{k_x, k_y}^*(x, y) \\
&= \frac{\alpha}{C} \sum_{k_x=1}^K \sum_{k_y=1}^K \frac{1}{K^2} \text{be}(x|k_x, K - k_x + 1) \text{be}(y|k_y, K - k_y + 1) = \frac{\alpha}{C}
\end{aligned}$$

In step 2, we use the fact that S_{k_x, k_y}^* is the overlap between the $K \times K$ unit square partition set S_{k_x, k_y} and the irregular domain \mathcal{D} , and will have area either exactly equal to $1/K^2$, when $S_{k_x, k_y}^* = S_{k_x, k_y}$, or area that can be approximated by $1/K^2$. In step 4, we use the fact that $B_{k_x, k_y} \approx 0$ for $(k_x, k_y) \notin J_K$.

B Appendix: Posterior simulation details

B.1 Temporal NHPP models

Here we give posterior simulation details for model (2) in section 2.1. Given the number of basis K , the Markov Chain Monte Carlo algorithm consists of Gibbs or Metropolis update from the full conditionals for ξ_i , V_k and α .

1. $\xi_i \mid -$

$$p(\xi_i = j \mid -) = \frac{V_j \text{be}(s|j, K - j + 1)}{\sum_{l=1}^K V_l \text{be}(s|l, K - l + 1)}$$

2. $V_k|-$ for $k = 1 \cdots K$, $M_k = \sum_{i=1}^n \delta_k(\xi_i)$

$$p(V_k|-) \propto \exp(-V_k) V_k^{M_k} V_k^{\alpha/K-1} \exp(-C V_k) \propto \text{ga}(V_k | M_k + \alpha/K, C + 1)$$

3. $\alpha|-$

$$\begin{aligned} p(\alpha|-) &\propto \text{ga}(\alpha | a_\alpha, b_\alpha) \prod_{k=1}^K \text{ga}(V_{k_x, k_y} | \alpha K^{-1}, C) \\ &\propto \alpha^{a_\alpha-1} \exp(-b_\alpha \alpha) C^\alpha \Gamma(\alpha/K)^{-K} \prod_{k=1}^K V_k^{\alpha/K} \end{aligned}$$

A metropolis step is implemented on the log scale with a normal random walk proposal density to sample from this full conditional.

The Markov Chain Monte Carlo algorithm for the density formulation of the temporal Poisson process under model (3) in section 2.1 consists of either a Metropolis or a Gibbs update from the following full-conditionals:

Let $k(s|\theta) = \sum_{k=1}^K \mathbb{1}_{((k-1)/K, k/K)}(\theta) \text{be}(s|k, K - k + 1)$

1. $\theta_i | \boldsymbol{\theta}_{-i}, -$

$$\begin{aligned} p(\theta_i | \boldsymbol{\theta}_{-i}, -) &= \frac{\alpha q_0}{\alpha q_0 + H} \frac{k(s_i | \theta) f_0(\theta)}{q_0} + \frac{1}{\alpha q_0 + H} \sum_{j=1}^{n^{*-}} k(s_i | \theta_j^{*-}) n_j^- \delta_{\theta_j^{*-}}(\theta_i) \\ q_0 &= \int k(s_i | \theta) f_0(\theta) d\theta = \sum_{j=1}^K \text{be}(s_i | j, K - j + 1) \alpha / K \\ H &= \sum_{j=1}^{n^{*-}} k(s_i | \theta_j^{*-}) n_j^- \end{aligned}$$

where n^{*-} is the number of unique values, $\{\theta_j^{*-} : j = 1 \cdots n^{*-}\}$ is the vector of unique values, and $\{n_j^-, j = 1 \cdots n^{*-}\}$ the vector of the number of observations that take value θ_j^{*-} in the vector $\boldsymbol{\theta}_{-i} = \{\theta_l : l \neq i\}$.

2. $\Lambda|-$

$$\Lambda|- \sim \text{Ga}(\alpha + n, C + 1)$$

where n is the number of points

3. $\alpha|-$

$$\begin{aligned} p(\alpha|-) &\propto \left(\prod_{m=1}^n (\alpha + m - 1) \right)^{-1} \alpha^{n^*} \text{ga}(\Lambda | \alpha, C) \text{ga}(\alpha | a_0, b_0) \\ &\propto \left(\prod_{m=1}^n (\alpha + m - 1) \right)^{-1} \alpha^{n^*} \frac{C^\alpha}{\Gamma(\alpha)} \Lambda^{\alpha-1} \alpha^{a_0-1} \exp(-b_0 \alpha) \end{aligned}$$

A metropolis step is implemented with a normal proposal on the log scale.

4. $K|-$

$$p(K|-) \propto \prod_{i=1}^n \left\{ \sum_{k=1}^K \mathbb{1}_{[\frac{k-1}{K}, \frac{k}{K}]}(\theta_i) \text{be}(s_i|k, K-k+1) \right\} \pi(K|\{K_{min}, \dots, K_{max}\})$$

The full conditional for K is a discrete distribution and can be directly sampled from.

With each draw in the posterior sample for $\{(\theta_1 \dots \theta_n), \alpha, K\}$, we sample $\{\omega_k : k = 1 \dots K\}$ from the following Dirichlet distribution

$$\{\omega_k : k = 1 \dots K\} \sim \text{Dir}(\{\alpha/K + \sum_{i=1}^n \mathbb{1}_{[\frac{k-1}{K}, \frac{k}{K}]}(\theta_i) : k = 1 \dots K\})$$

We obtain a draw from the posterior distribution of the intensity function $\lambda(s)$ and the density function $f(s)$ evaluated at location s respectively, given $\{\omega_1, \dots, \omega_K\}$ via the following functions

$$\begin{aligned} f(s) &= \sum_{k=1}^K \omega_k \text{be}(s|k, K-k+1) \\ \lambda(s) &= \Lambda \sum_{k=1}^K \omega_k \text{be}(s|k, K-k+1) \end{aligned}$$

B.2 The intensity formulation for spatial NHPP over irregular domain

The full hierarchical model for the intensity formulation over irregular domain under (8) in section 3.1

$$\begin{aligned} \{(x_i, y_i)\} | \mathbf{V}, \{(\xi_i, \eta_i)\} &\sim \left(\prod_{k_x, k_y=1}^K \exp(-V_{k_x, k_y} B_{k_x, k_y}) \right) \prod_{i=1}^n \Lambda_{\mathcal{D}} \phi_{\xi_i, \eta_i}^*(x_i, y_i) \\ (\xi_i, \eta_i) | \mathbf{V} &\stackrel{i.i.d.}{\sim} \sum_{k_x, k_y=1}^K \frac{V_{k_x, k_y} B_{k_x, k_y}}{\Lambda_{\mathcal{D}}} \delta_{(k_x, k_y)}(\xi_i, \eta_i), \quad i = 1, \dots, n \\ \alpha, \mathbf{V} &\sim \text{Ga}(\alpha | a_\alpha, b_\alpha) \prod_{k_x, k_y=1}^K \text{Ga}(V_{k_x, k_y} | \alpha K^{-2}, C) \end{aligned}$$

where $\mathbf{V} = \{V_{k_x, k_y} : k_x, k_y = 1, \dots, K\}$, $\Lambda_{\mathcal{D}} = \sum_{k_x, k_y=1}^K V_{k_x, k_y} B_{k_x, k_y}$, and $B_{k_x, k_y} = \int \int_D \text{be}(x|k_x, K-k_x+1) \text{be}(y|k_y, K-k_y+1) dx dy$. $\{B_{k_x, k_y}, k_x, k_y = 1 \dots K\}$ can be computed given K and \mathcal{D} before running the Markov Chain Monte Carlo algorithm to save computation time.

Given the number of basis K , the Markov Chain Monte Carlo algorithm consists of Gibbs or Metropolis update from the full conditionals for $\{\xi_i, \eta_i\}$, V_{k_x, k_y} and α :

1. The full conditional for $\{\xi_i, \eta_i\}$ are discrete distributions

$$p(\xi_i = m, \eta_i = n|-) = \frac{V_{m,n} \text{be}(x_i|m, K-m+1) \text{be}(y_i|n, K-n+1)}{\sum_{p,q=1}^K V_{p,q} \text{be}(x_i|p, K-p+1) \text{be}(y_i|q, K-q+1)}$$

2. The full conditional for $V_{k_x, k_y}, k_x, k_y = 1 \dots K$ are independent Gamma distributions, which can be sampled directly from in a vectorized fashion. Let M_{k_x, k_y} be the number of latent variable pairs (ξ_i, τ_i) in step 1 that take value (k_x, k_y) .

$$\begin{aligned}
p(V_{k_x, k_y} | -) &\propto \exp(-V_{k_x, k_y} B_{k_x, k_y}) \prod_{i=1}^n \Lambda_{\mathcal{D}} \sum_{k_x, k_y=1}^K \frac{V_{k_x, k_y} B_{k_x, k_y}}{\Lambda_{\mathcal{D}}} \delta_{(k_x, k_y)}(\xi_i, \eta_i) \phi_{k_x, k_y}^*(x_i, y_i) \\
&\quad \times \text{ga}(V_{k_x, k_y} | \alpha / K^2, C) \\
&\propto \exp(-V_{k_x, k_y} B_{k_x, k_y}) \prod_{i=1}^n (V_{k_x, k_y} B_{k_x, k_y})^{\delta_{(k_x, k_y)}(\xi_i, \eta_i)} \text{ga}(V_{k_x, k_y} | \alpha / K^2, C) \\
&\propto \text{ga}(V_{k_x, k_y} | M_{k_x, k_y} + \alpha / K^2, C + B_{k_x, k_y})
\end{aligned}$$

3. The full conditional for α is

$$\begin{aligned}
p(\alpha | -) &\propto \text{ga}(\alpha | a_\alpha, b_\alpha) \prod_{k_x, k_y=1}^K \text{ga}(V_{k_x, k_y} | \alpha K^{-2}, C) \\
&\propto \alpha^{a_\alpha - 1} \exp(-b_\alpha \alpha) C^\alpha \Gamma(\alpha / K^2)^{-K^2} \prod_{k_x, k_y=1}^K V_{k_x, k_y}^{\alpha K^{-2}}
\end{aligned}$$

A metropolis step is implemented on the log scale with a normal random walk proposal density to sample from this full conditional.

B.3 The density formulation for spatial NHPP over irregular domain

The full hierarchical model for the density formulation over irregular domain under model (11) in section 3.2 is

$$\begin{aligned}
\{(x_i, y_i)\} | \{\mathbf{z}_i\}, \Lambda_{\mathcal{D}}, K &\sim \exp(-\Lambda_{\mathcal{D}}) \prod_{i=1}^n \Lambda_{\mathcal{D}} \sum_{k_x, k_y \in J_k} \mathbb{1}_{S_{k_x, k_y}^*}(\mathbf{z}_i) \phi_{k_x, k_y}^*(x_i, y_i) \\
(x_i, y_i), \mathbf{z}_i \in \mathcal{D}, \mathbf{z}_i &| F \stackrel{i.i.d.}{\sim} F, \quad i = 1 \dots, n \\
F | \alpha &\sim \text{DP}(\alpha, F_0) \quad F_0(\cdot) \equiv \text{Unif}(\mathcal{D}) \\
\Lambda_{\mathcal{D}} | \alpha &\sim \text{Ga}(\alpha, C) \quad \alpha \sim \text{Ga}(\alpha | a_\alpha, b_\alpha) \quad K \sim \pi(K | \{K_{\min}, \dots, K_{\max}\})
\end{aligned}$$

The Markov Chain Monte Carlo algorithm consists of either Metropolis or Gibbs update from the following full-conditionals:

1. $\mathbf{z}_i | \mathbf{z}_{-i}, \alpha, K$, where \mathbf{z}_i is the bivariate continuous latent variable.

Let $k^*(\mathbf{s}_i | \mathbf{z}_i) = \sum_{(k_x, k_y) \in J_k} \mathbb{1}_{S_{k_x, k_y}^*}(\mathbf{z}_i) W_{k_x, k_y, i}^*$, where $W_{k_x, k_y, i}^* = \phi_{k_x, k_y}^*(x_i, y_i)$ is a constant.

$$\begin{aligned}
p(\mathbf{z}_i | \mathbf{z}_{-i}, \mathbf{s}_i) &= \frac{\alpha q_0}{\alpha q_0 + H} \frac{k^*(\mathbf{s}_i | \mathbf{z}) f_0(\mathbf{z})}{q_0} + \frac{1}{\alpha q_0 + H} \sum_{j=1}^{n^*} k^*(\mathbf{s}_i | \mathbf{z}_j^{*-}) n_j^- \delta_{\mathbf{z}_j^{*-}}(\mathbf{z}_i) \\
&= \frac{\alpha q_0}{\alpha q_0 + H} q(\mathbf{z} | \mathbf{s}_i) + \frac{1}{\alpha q_0 + H} \sum_{j=1}^{n^*} k^*(\mathbf{s}_i | \mathbf{z}_j^{*-}) n_j^- \delta_{\mathbf{z}_j^{*-}}(\mathbf{z}_i) \\
q_0 &= \int k^*(\mathbf{s}_i | \mathbf{z}) f_0(\mathbf{z}) d\mathbf{z} = \sum_{(k_x, k_y) \in J_k} W_{k_x, k_y, i}^* | S_{k_x, k_y}^* | / | \mathcal{D} | \\
q(\mathbf{z} | \mathbf{s}_i) &= \sum_{(k_x, k_y) \in J_k} W_{k_x, k_y, i}^* q_0^{-1} \mathbb{1}_{S_{k_x, k_y}^*}(\mathbf{z}) | \mathcal{D} |^{-1} \\
&= \sum_{(k_x, k_y) \in J_k} \frac{W_{k_x, k_y, i}^* | S_{k_x, k_y}^* |}{\sum_{m, n} W_{m, n, i}^* | S_{k_x, k_y}^* |} \mathbb{1}_{S_{k_x, k_y}^*}(\mathbf{z}) | S_{k_x, k_y}^* |^{-1} \\
H &= \sum_{j=1}^{n^*} k^*(\mathbf{s}_i | \mathbf{z}_j^{*-}) n_j^-
\end{aligned}$$

where n^{*-} is the number of unique values, $\{z_j^{*-} : j = 1 \cdots n^{*-}\}$ is the vector of unique values, and $\{n_j^-, j = 1 \cdots n^{*-}\}$ is the vector of the number of observations that take value z_j^{*-} in the vector $\mathbf{z}_{-i} = \{z_l : l \neq i\}$.

2. $\Lambda_{\mathcal{D}}|-$

$$\Lambda_{\mathcal{D}}|- \sim \text{Ga}(\alpha + n, C + 1)$$

where n is number of points.

3. $\alpha|-$

$$\begin{aligned} p(\alpha|-) &\propto \left(\prod_{m=1}^n (\alpha + m - 1) \right)^{-1} \alpha^{n^*} \text{ga}(\Lambda_{\mathcal{D}}|\alpha, C) \text{ga}(\alpha|a_0, b_0) \\ &\propto \left(\prod_{m=1}^n (\alpha + m - 1) \right)^{-1} \alpha^{n^*} \frac{C^\alpha}{\Gamma(\alpha)} \Lambda_{\mathcal{D}}^{\alpha-1} \alpha^{a_0-1} \exp(-b_0\alpha) \end{aligned}$$

A metropolis step is implemented with a normal proposal on the log scale.

4. $K|-$

$$p(K|-) \propto \prod_{i=1}^n \left\{ \sum_{k_x, k_y \in J_K} \mathbb{1}_{S_{k_x, k_y}^*}(\mathbf{z}_i) W_{k_x, k_y, i}^* \right\} \pi(K|\{K_{min}, \dots, K_{max}\})$$

The full conditional for K is a discrete distribution and can be directly sample from.

With each draw in the posterior sample for $\{\Lambda_{\mathcal{D}}, \{\mathbf{z}_i\}, \alpha, K\}$, we obtain a draw from the posterior distribution of $\{\omega_{k_x, k_y}^* : (k_x, k_y) \in J_K\}$ by sampling from the following Dirichlet distribution:

$$\{\omega_{k_x, k_y}^* : k_x, k_y = 1 \cdots K\} \sim \text{Dir}(\{\alpha/ | S_{k_x, k_y}^* | + \sum_{i=1}^n \mathbb{1}_{S_{k_x, k_y}^*}(\mathbf{z}_i) : k_x, k_y = 1 \cdots K\})$$

We obtain a draw from the posterior distribution of the intensity function $\lambda_{\mathcal{D}}(\mathbf{s})$ and the density function $f_{\mathcal{D}}(\mathbf{s})$ evaluated at location $\mathbf{s} = (x, y)$ respectively, given $\{\omega_{k_x, k_y}^* : k_x, k_y = 1 \cdots K\}$, via the following function

$$\begin{aligned} f_{\mathcal{D}}(x, y) &= \sum_{(k_x, k_y) \in J_K} \omega_{k_x, k_y}^* \phi_{k_x, k_y}^*(x, y) \\ \lambda_{\mathcal{D}}(x, y) &= \Lambda_{\mathcal{D}} \sum_{(k_x, k_y) \in J_K} \omega_{k_x, k_y}^* \phi_{k_x, k_y}^*(x, y) \end{aligned}$$